Supplementary Information

Structural engineering of Pt-on-Rh hollow nanorods with high-performance peroxidase-like specific activity for colorimetric detection

*Jian Hao,‡ Yi Tan,‡ Jincheng Yuan, Rui Shang, Dong Xiang and Kai Cai**

College of Chemistry & Environmental Engineering, Yangtze University, Jingzhou 434100, China

*Corresponding Author.

E-mail: caikai2000@163.com (K.C.)

Chemicals

Tellurium dioxide powder (TeO_2, 99.99%), and selenous acid (H_2SeO_3, 99.99%) were purchased from Aladdin Chemistry Co., Ltd. Hydrazine monohydrate (N_2H_4 H_2O, 85%, AR), sodium dodecyl sulfate (SDS, 99%), chloroplatinic acid (H_2PtCl_6 $6H_2O$ AR), rhodium chloride hydrate ($RhCl_3$ $3H_2O$), polyvinylpyr-rolidone (PVP10 Average molecular weight 58000 AR), hydrogenperoxide (H_2O_2, 30%, AR) were provided by Sinopharm Chemical Reagent Co., Ltd. 3,3',5,5' tetramethylbenzidine (TMB), Citric acid/sodium was obtained from McLean chemical reagent Co., Ltd.

Instruments

Transmission electron microscopy (TEM) imaging was measured on a FEI TECNAI F30 microscope operated at 200 kV and copper grids were used to load the samples. X-ray spectroscopy (EDS) was conducted under the high-angle annular dark field (HAADF) mode with an EDAX attachment. Inductively coupled plasma-mass spectrometry (ICP-MS) measurements were performed on NexION 300Q (PerkinElmer, USA). X-ray diffraction (XRD) was tested on a Bruker D8 Advance X-ray diffractometer with Cu Kα radiation. Samples were prepared by depositing nanostructures on glass. The scanning speed was set as 15 degrees/min. X-ray photoelectron spectra (XPS) were collected on an ESCALAB 250Xi spectrophotometer (Thermo Fisher) with Al Kα X-ray radiation and calibrated using the C 1s peak (284.8 eV). UV-vis-NIR spectra were measured by a Lambda 750UV-vis-NIR spectrophoto meter (PerkinElmer, USA).

Evaluation of Peroxidase-like Activity and Kinetic Parameters of PtRh HNRs

Specific activity (SA) was measured according to the protocol reported in former reports.[1] Specifically, at 25 ℃, 0.1 M citric acid/sodium citrate was selected as buffer (pH=4.0). H_2O_2, nanozyme material, TMB (50 μL 10 mg/mL) were added successively. The final volume is controlled at 1 mL, in which the concentration of H_2O_2 is 1.0 M, and the mass of nanozyme material added each time is controlled. The absorbance of the reaction solution at λ_{max}=653 nm was measured by UV-vis spectrophotometer at the interval of 1 second immediately after the addition of all substances for 50 s. The absorbance-time curve is then obtained and SA is calculated by the following equation.

$$b_{nanozyme} = \frac{V}{\varepsilon l} \times \frac{\Delta A}{\Delta t}$$

where $b_{nanozyme}$ is the nanozyme activity (U), V is the total volume of reaction solution (μL), ε is the molar absorption coefficient of the TMB substrate (39,000 M^{-1} cm^{-1} at 653 nm), l is the optical path length through reaction solution (cm), and ΔA/Δt is the initial rate of the absorbance change (min^{-1}). When using different amounts of the nanozyme to measure the peroxidase-like activity, the specific activity of the nanozyme was determined using the following equation:

$$SA = \frac{b_{nanozyme}}{m}$$

where SA is the specific activity of the nanozyme (U mg^{-1}), and m is the nanozyme amount (mg).

Peroxidase-like activities of the nanozyme material were evaluated by the steady-state kinetic assays, according to the previous report.[2] Specifically, 0.1 M citric acid/sodium citrate were added successively as buffer (pH=4.0). H_2O_2, nanozyme material (50 μL, 2 mg/L) and TMB were added in the cuvette (path length, 1.0 cm) at 25 ℃. The final volume is controlled at 1 mL, in which the concentration of H_2O_2 is 2.0 M, and TMB is controlled as the variable. After

adding all substances, the absorbance of the reaction solution at λ_{max}=653 nm was measured by UV-vis spectrophotometer at an interval of 2 seconds for 50 s. Then, the absorbance and time curve is obtained, from which the initial reaction rate is calculated and the maximum reaction rate V_{max} and the Michaelis constant (K_m) are accessed by the Michaelis-Menten equation.

$$V = \frac{V_{max}[S]}{K_m + [S]}$$

where V_{max} is the maximal reaction velocity, [S] is the concentration of TMB, and K_m is the Michaelis constant. The values of K_m and V_{max} can be obtained from the double reciprocal plots.

Stability test process:

Specifically, at 25 ℃, 0.1 M citric acid/sodium citrate was selected as buffer (pH=4.0). H_2O_2, nanozyme material, TMB (50 μL 10 mg/mL) were added successively. The final volume is controlled at 1 mL, in which the concentration of H_2O_2 is 1.0 M, and the mass of nanozyme material added each time is controlled. The absorbance of the reaction solution at λ_{max}=653 nm was measured by UV-vis spectrophotometer after the addition of all substances for 50 s. The same procedure was used every day for ten days.

Isopropanol quenching hydroxyl radical test process

Typically, 50 μL isopropanol, 50 μL TMB (10 mg/mL), 50 μL H_2O_2 with different concentrations and 50 μL nanozyme (2 mg/L) were added to sodium citrate (0.1 M, pH=4.0). The final volume is controlled at 1 mL, after adding all substances, the absorbance of the reaction solution at λ_{max}=653 nm was measured by UV-vis spectrophotometer at an interval of 1 seconds for 40 s.

Colorimetric determination of H_2O_2 and ascorbic acid (AA)

The steps for the determination of H_2O_2 and AA are based on the previously reported methods.[3] In simple terms, for H_2O_2 detection, 50 μL TMB (10 mg/mL) and PtRh nanorods (50 μL, 2 mg/L) were added to 850 μL sodium citrate solution (0.1 M, pH=4.0). Then, 50 μL H_2O_2 with different concentrations was added, after incubation for 1 min, tested the solution by UV-vis spectroscopy. For AA detection, added 50 μL TMB (10 mg/mL), PtRh-3 HNRs (50 μL, 2 mg/L), H_2O_2 (50 μL, 10 mM), 50 μL ascorbic acid with different concentrations was added to 800 μL sodium citrate solution (0.1 M, pH=4.0).

Determination of vitamin C tablets

Three solutions of commercial vitamin C samples were prepared respectively firstly. Then the presupposed concentration of ascorbic acid of the samples was obtained according to the specifications and the concentration of 0.02 mM was used in the test. The colorimetric detection process was similar to the method of the determination of AA using PtRh-3 HNRs. Finally, AA contents of the commercial samples were calculated through absorbance values at 653 nm and the AA standard curve.

Theoretical calculations

The Vienna Ab Initio Package (VASP) was employed to perform all the density functional theory (DFT) calculations within the generalized gradient approximation (GGA) using the Perdew, Burke, and Enzerhof (PBE) formulation.[4-6] The projected augmented wave (PAW) potentials were applied to describe the ionic cores and take valence electrons into account using a plane wave basis set with a kinetic energy cutoff of 450 eV.[7,8] Partial occupancies of the Kohn–Sham orbitals were allowed using the Gaussian smearing method and a width of 0.05 eV. The electronic energy was considered self-consistent when the energy change was smaller than 10^{-5} eV. A geometry optimization was considered convergent when the force change was smaller

than 0.05 eV/Å. Grimme's DFT-D3 methodology was used to describe the dispersion interactions.[9] The vacuum spacing perpendicular to the plane of the structure is 20 Å. The Brillouin zone integral utilized the surfaces structures of 2×2×1 monkhorst pack K-point sampling. The Charge density difference of system: $\Delta\rho = \rho_{total} - \rho_A - \rho_B$, where ρ_{total} is the charge density of Binding systems, ρ_A and ρ_B is the sub charge density. Finally, the adsorption energies (E_{ads}) were calculated as $E_{ads} = E_{ad/sub} - E_{ad} - E_{sub}$, where $E_{ad/sub}$, E_{ad}, and E_{sub} are the total energies of the optimized adsorbate/substrate system, the adsorbate in the structure, and the clean substrate, respectively. The free energy was calculated using the equation:

$G = E_{ads} + ZPE - TS$

where G, E_{ads}, ZPE and TS are the free energy, total energy from DFT calculations, zero point energy and entropic contributions, respectively.

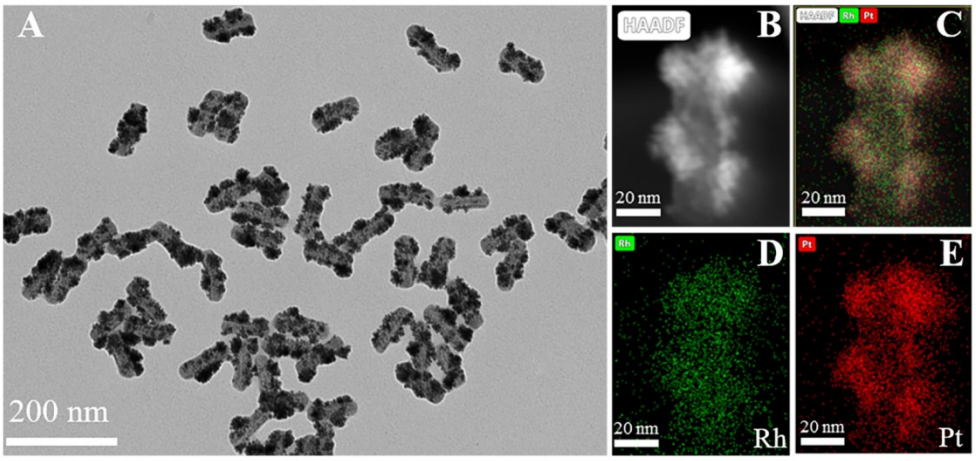

Figure S1. TEM image (A), and EDS mapping images (B-E) of PtRh-2 HNRs.

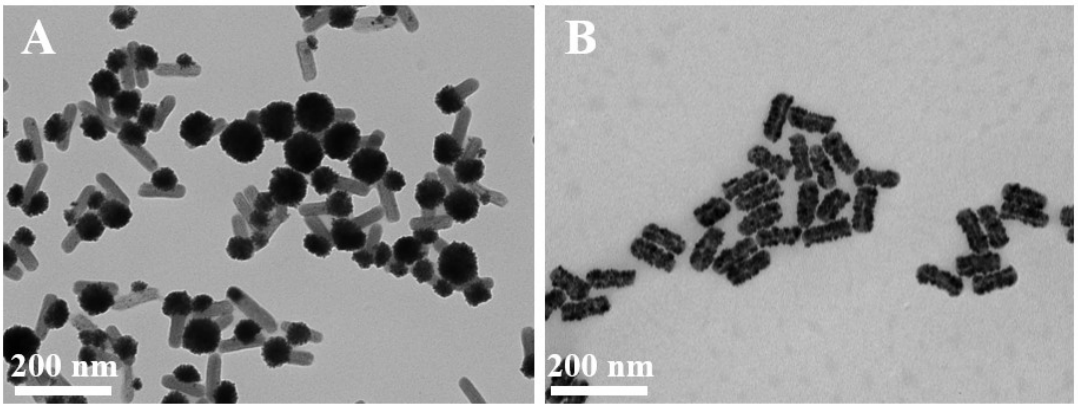

Figure S2. TEM images of PtRh HNRs prepared at different PVP concentrations. (A) 1 μg mL^{-1}, PtRh-1 HNRs, (B) 5000 μg mL^{-1}, PtRh-4 HNRs.

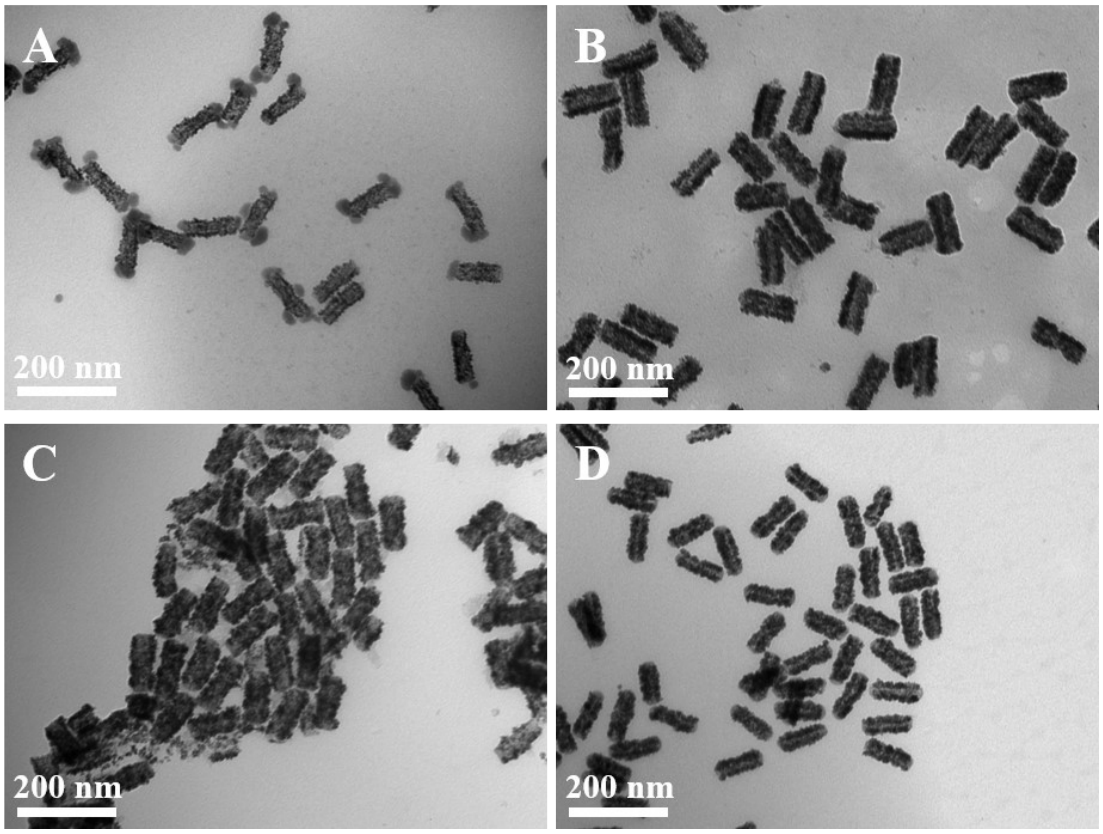

Figure S3. TEM images of Pt HNRs prepared at different PVP concentrations. (A) 1 μg mL^{-1}, (B) 50 μg mL^{-1}, (C) 500 μg mL^{-1}, (D) 5000 μg mL^{-1}.

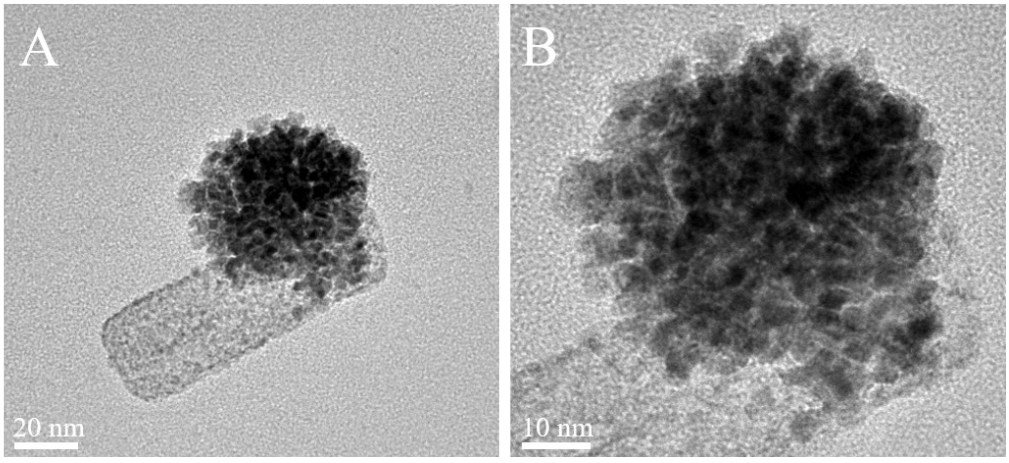

Figure S4. (A, B) HRTEM images of PtRh-1 HNRs.

Table S1. The fitting data of XPS.

	4f	BE	Lorentzian /gaussian	FWHM
Pt	Pt4f7/2	71.15	99.93	0.83
	Pt4f5/2	74.35	99.93	0.83
PtRh-1	Pt4f7/2	70.95	99.98	0.85
	Pt4f5/2	74.29	99.98	0.85
PtRh-3	Pt4f7/2	70.86	99.91	0.88
	Pt4f5/2	74.15	99.91	0.88

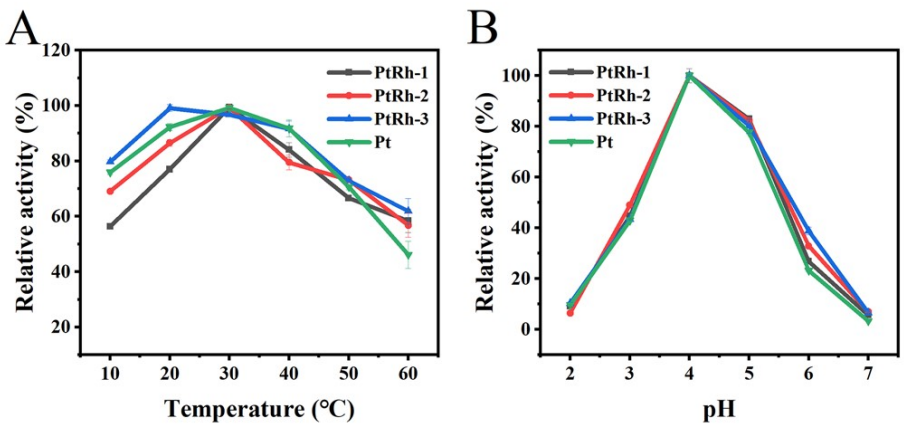

Figure S5. Influence of pH (A), and temperature (B) on the peroxidase-like activity of the nanozymes. The maximum value in each curve is set as 100%.

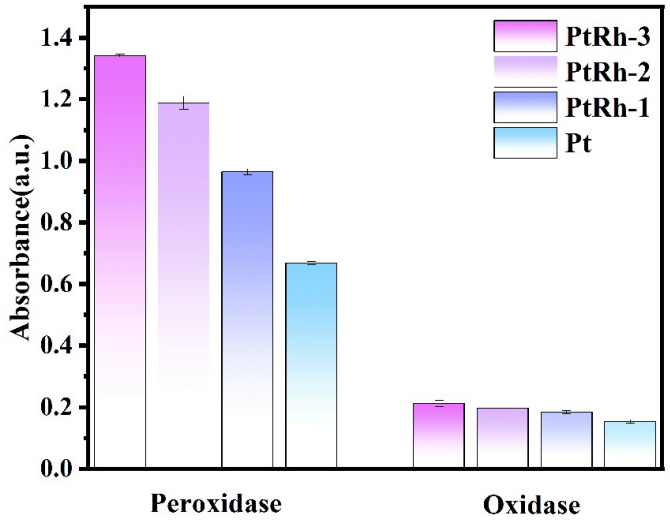

Figure S6. Comparison of POD-like and OXD-like activities of different nanozymes.

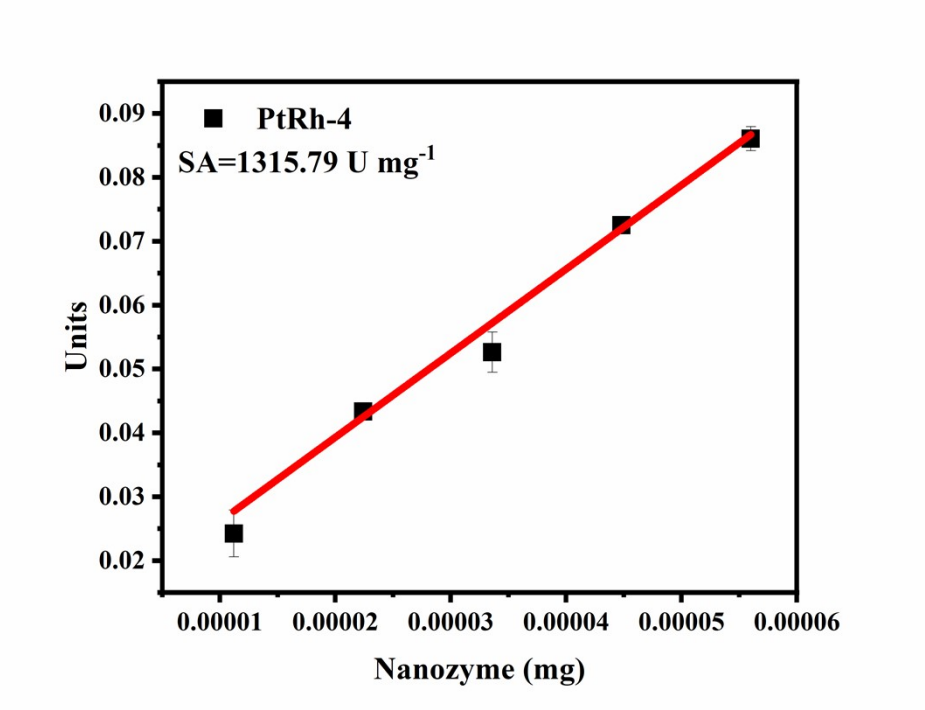

Figure S7. The SA values of PtRh-4 HNRs.

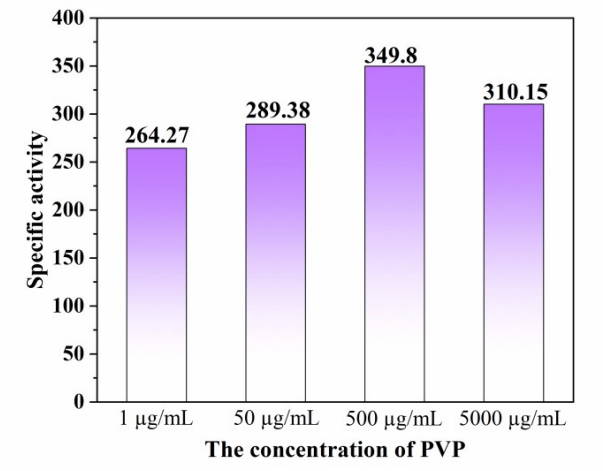

Figure S8. The SA values of Pt nanorods obtained in different PVP concentrations.

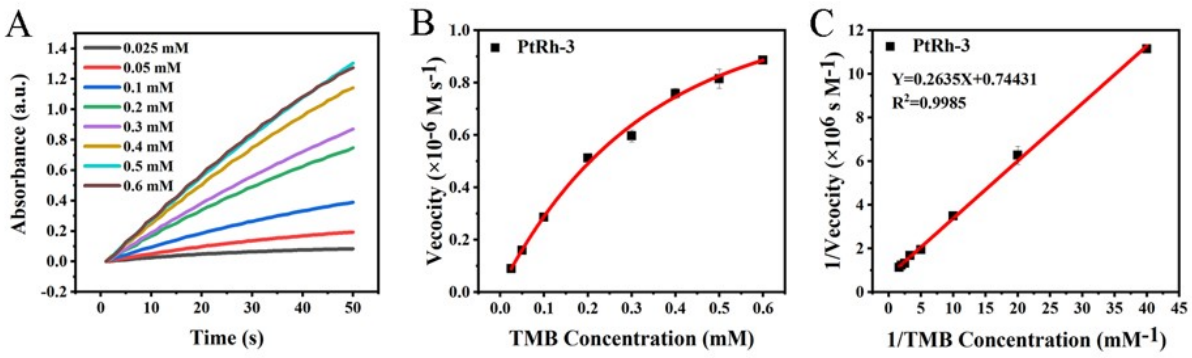

Figure S9. (A) Time-absorbance curves obtained from different TMB concentrations using PtRh-3 HNRs in system. (B) Initial reaction velocity against TMB concentration. (C) Double-reciprocal plots for the reaction velocity against TMB concentration.

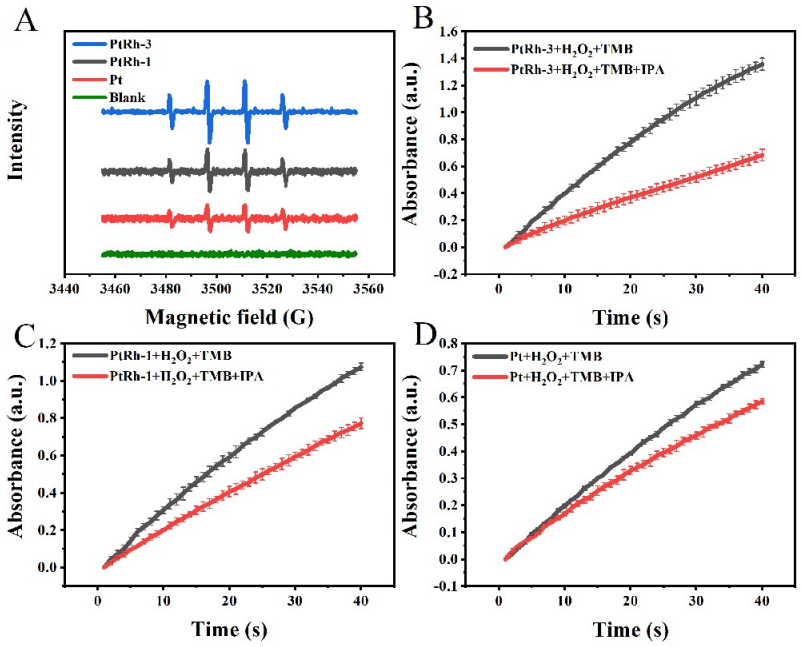

Figure S10. (A) EPR spectra of reaction systems using H_2O_2 + nanozyme at 5 min. Time-absorbance curves of reaction systems with isopropanol (IPA) added or not under different nanozymes: (B) PtRh-3 HNRs, (C) PtRh-1 HNRs, (D) Pt HNRs.

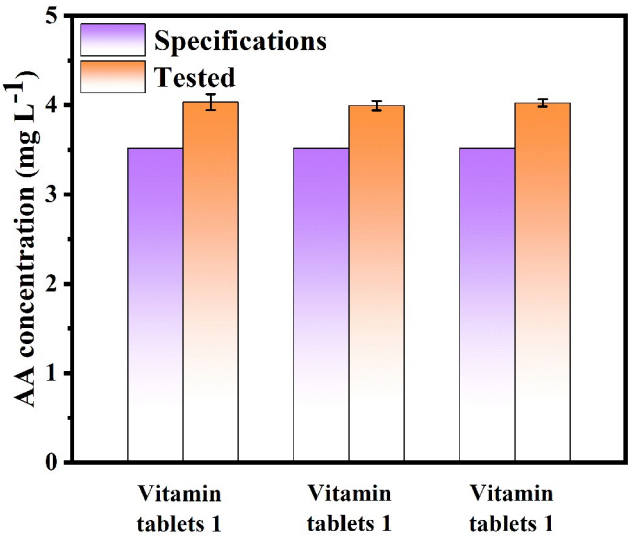

Figure S11. AA concentration of commercial vitamin C tablets measured by colorimetric detection in comparison with their specifications.

Table S2. The ICP test of PtRh-4, PtRh-3, PtRh-2, PtRh-1 and Pt HNRs.

	Rh (μg/L)	Pt (μg/L)	Rh/Pt ratio
PtRh-4	0.5704	12.38	0.04607
PtRh-3	0.6829	14.72	0.04639
PtRh-2	0.5925	10.62	0.05579
PtRh-1	0.8821	15.03	0.05869
Pt		18.55	

Table S3. The specific activities of nanozymes.

	Substrate	SA(U mg^{-1})	ref
HG-Heme	TMB	67.3	10
FeNCP/NW	TMB	86.9	11
PdPtAu alloy	TMB	81.245	12
A-Ru	TMB	164.46	13
Os NPS	TMB	393	14
USPBNPS	TMB	465.8	15
FeN_3P-Sazyme	TMB	316	16
Natural HRP	TMB	1305	17
H-Pt_3Sn	TMB	345.32	18
PtPdAu	TMB	563.71	19
PtRh-4	TMB	1315.8	This work
PtRh-3	TMB	1352.2	This work
PtRh-2	TMB	892.7	This work
PtRh-1	TMB	607.6	This work
Pt	TMB	349.8	This work

Table S4. Comparison of limit of detection of H_2O_2 using different nanozymes.

Nanozymes	Signal type	Detection range(μM)	Limit of detection(μM)	Reference
PdIr aerogels	Colorimetry	1-500	0.8	4
PtPdAu	Colorimetry	1-500	1.8	19
MIL-88	Colorimetry	2-20.3	0.562	20
Co_3O_4 NPs	Colorimetry	50-25000	10	21
Hemin@MOF	Colorimetry	5-200	2	22
GO-COOH	Colorimetry	0.05-1	0.05	23
C-Dots	Colorimetry	1-100	0.2	24
WS_2	Colorimetry	10-100	1.2	25
Hemin/WS_2-NSs	Colorimetry	5-140	1.0	26
MIL-53(Fe)	Colorimetry	0.95-19	0.13	27
PtRh-3	Colorimetry	1-500	9.97	This work

Table S5. Comparison of limits of detection of AA using different nanozymes.

Nanozymes	Signal type	Detection range	Limit of detection	Reference
PdIr aerogels	Colorimetry	0.5-250 μM	0.22 μM	4
PtPdAu	Colorimetry	1-50 μM	0.068 μM	19
MIL-88	Colorimetry	2.57-10.1 μM	1 μM	20
Au/RGO	Electrochemistry	0.24-1.5 mM	0.05 mM	28
Pt–Ni alloy	Electrochemistry	0.57-5.7 mM	0.33 mM	29
PPF	Electrochemistry	0.4-6 mM	0.12 mM	30
ERGO	Electrochemistry	0.5-2 mM	0.3 mM	31
SNC-900	Colorimetry	0.1-5 mM	80 μM	32
Au/Cu NRs	Colorimetry	0-2 mM	25 μM	33
PtRh-3	Colorimetry	1-25 μM	0.039μM	This work

REFERENCES

(1) B. Jiang, D. Duan, L. Gao, M. Zhou, K. Fan, Y. Tang, J. Xi, Y. Bi, Z. Tong, G. F. Gao, N. Xie, A. Tang, G. Nie, M. Liang and X. Yan, *Nat. Protoc*., 2018, **13**, 1506-1520.
(2) Z. Xi, K. Wei, Q. Wang, M. J. Kim, S. Sun, V. Fung and X. Xia, *J. Am. Chem. Soc*., 2021, **143**, 2660-2664.
(3) X. Tan, Q. Yang, X. Sun, P. Sun and H. Li, *ACS Appl. Mater. Interfaces*, 2022, **14**, 10047-10054.
(4) G. Kresse and J. Furthmüller, *Phys. Rev. B.*, 1996, **54**, 11169-11186.
(5) J. P. Perdew, K. Burke and M. Ernzerhof, *Phys. Rev. Lett.*, 1996, **77**, 3865-3868.
(6) G. Kresse and D. Joubert, *Phys. Rev. B.*, 1999, **59**, 1758-1775.
(7) P. E. Blöchl, *Phys. Rev. B.*, 1994, **50**, 17953-17979.
(8) S. Grimme, J. Antony, S. Ehrlich and H. Krieg, *J. Chem. Phys.*, 2010, **132**, 154104.
(9) G. Henkelman, B. P. Uberuaga and H. Jónsson, *J. Chem. Phys.*, 2000, **113**, 9901-9904.
(10) W. Xu, W. Song, Y. Kang, L. Jiao, Y. Wu, Y. Chen, X. Cai, L. Zheng, W. Gu and C. Zhu, *Anal. Chem*., 2021, **93**, 12758-12766.
(11) S. Ding, J. A. Barr, Z. Lyu, F. Zhang, M. Wang, P. Tieu, X. Li, M. H. Engelhard, Z. Feng, S. P. Beckman, X. Pan, J.-C. Li, D. Du and Y. Lin, *Adv. Mater*., 2024, **36**, 2209633.
(12) L. Huang, Y. Zhou, Y. Zhu, H. Su, S. Yang, L. Feng, L. Zhao, S. Liu and K. Qian, *Biosens. Bioelectron.*, 2022, **210**, 114254.
(13) Y. Tang, Y. Wu, W. Xu, L. Jiao, Y. Chen, M. Sha, H.-R. Ye, W. Gu and C. Zhu, *Anal. Chem*., 2022, **94**, 1022-1028.
(14) S. He, L. Yang, P. Balasubramanian, S. Li, H. Peng, Y. Kuang, H. Deng and W. Chen, *J. Mater. Chem. A*., 2020, **8**, 25226-25234.
(15) Z. Qin, B. Chen, Y. Mao, C. Shi, Y. Li, X. Huang, F. Yang and N. Gu, *ACS Appl. Mater. Interfaces*, 2020, **12**, 57382-57390.
(16) S. Ji, B. Jiang, H. Hao, Y. Chen, J. Dong, Y. Mao, Z. Zhang, R. Gao, W. Chen, R. Zhang, Q. Liang, H. Li, S. Liu, Y. Wang, Q. Zhang, L. Gu, D. Duan, M. Liang, D. Wang, X. Yan and Y. Li, *Nat. Catal.*, 2021, **4**, 407-417.
(17) H. Fan, J. Zheng, J. Xie, J. Liu, X. Gao, X. Yan, K. Fan and L. Gao, *Adv. Mater.*, 2024, **36**, 2300387.
(18) Y. Tang, Y. Chen, Y. Wu, W. Xu, Z. Luo, H.-R. Ye, W. Gu, W. Song, S. Guo and C. Zhu, *Nano Lett.*, 2023, **23**, 267-275.
(19) Y. Tan, J. Yuan, R. Shang, J. Hao, S. Hu and K. Cai, *Dalton. Trans.*, 2024, **53**, 5624-5631.
(20) C. Gao, H. Zhu, J. Chen and H. Qiu, *Chinese Chem. Lett*., 2017, **28**, 1006-1012.
(21) J. Mu, Y. Wang, M. Zhao and L. Zhang, *Chem. Commun*., 2012, **48**, 2540-2542.
(22) F.-X. Qin, S.-Y. Jia, F.-F. Wang, S.-H. Wu, J. Song and Y. Liu, Catal. *Sci. Technol.*, 2013, **3**, 2761-2768.
(23) Y. Song, K. Qu, C. Zhao, J. Ren and X. Qu, *Adv. Mater*., 2010, 22, 2206-2210.
(24) W. Shi, Q. Wang, Y. Long, Z. Cheng, S. Chen, H. Zheng and Y. Huang, *Chem. Commun.*, 2011, **47**, 6695-6697.
(25) T. Lin, L. Zhong, Z. Song, L. Guo, H. Wu, Q. Guo, Y. Chen, F. Fu and G. Chen, *Biosens. Bioelectron.*, 2014, **62**, 302-307.
(26) Q. Chen, J. Chen, C. Gao, M. Zhang, J. Chen and H. Qiu, *Analyst*, 2015, **140**, 2857-2863.
(27) L. Ai, L. Li, C. Zhang, J. Fu and J. Jiang, *Chem–Eur. J*., 2013, **19**, 15105-15108.
(28) C. Wang, J. Du, H. Wang, C. e. Zou, F. Jiang, P. Yang and Y. Du, Sensor. *Actuat. B-Chem.*, 2014, **204**, 302-309.

(29) Y.-C. Weng, Y.-G. Lee, Y.-L. Hsiao and C.-Y. Lin, *Electrochim*. *Acta*, 2011, **56**, 9937-9945.
(30) G. P. Keeley, A. O'Neill, N. McEvoy, N. Peltekis, J. N. Coleman and G. S. Duesberg, *J. Mater. Chem.*, 2010, **20**, 7864-7869.
(31) L. Yang, D. Liu, J. Huang and T. You, *Sens. Actuators. B*., 2014, **193**, 166-172.
(32) Y. Chen, L. Jiao, H. Yan, W. Xu, Y. Wu, H. Wang, W. Gu and C. Zhu, *Analy. Chem*., 2020, **92**, 13518-13524.
(33) S. Xu, X. Dong, S. Chen, Y. Zhao, G. Shan, Y. Sun, Y. Chen and Y. Liu, *Sens. Actuators. B*., 2019, **281**, 375-382.